Spectro-angular analysis of roadside-integrated bifacial solar power systems with reflecting sound barriers

Journal of Physics: Photonics

PAPER

Spectro-angular analysis of roadside-integrated bifacial solar power systems with reflecting sound barriers

Silvi Bundo[1], Shweta Pal[1], Marco Ernst[2] and Rebecca Saive[1,*]

[1] Inorganic Materials Science, MESA+, University of Twente, Enschede 7522NB, The Netherlands
[2] School of Engineering, The Australian National University, Canberra, ACT 2600, Australia
* Author to whom any correspondence should be addressed.

E-mail: r.saive@utwente.nl

Keywords: spectro-angular irradiance, building integrated photovoltaics (BIPV), direct irradiance, diffuse irradiance

OPEN ACCESS

RECEIVED
15 September 2023

REVISED
12 February 2024

ACCEPTED FOR PUBLICATION
20 February 2024

PUBLISHED
14 March 2024

Abstract

Bifacial photovoltaic modules along highways provide energy supply and act as sound barriers simultaneously. This study examines the impact on energy production when incorporating sound barriers with varying light reflection properties into this integrated solar infrastructure along roadways. Specifically, we use advanced computational simulations to analyze the effects of integrating black, ideal specular, and ideal diffuse (Lambertian) reflectors into an existing highway solar power plant located in the Netherlands. Our analysis combines realistic spectro-angular irradiance data as input with our in-house reverse ray tracing software. Our calculations show that for an east-west facing system, an ideal diffuse reflector increases the annual yield by 70%, while a specular reflector decreases the yield due to shading. Most notably, the diffuse reflector doubles the energy yield during winter months, thereby offering a pathway to decrease the seasonal energy demand and supply gap.

1. Introduction

To meet the increasing demand of energy needs for densely populated countries, such as the Netherlands, we need novel building-integrated photovoltaic (BIPV) configurations [1]. Rooftops are the primary option, currently comprising almost 80% of the photovoltaic (PV) installations in the Netherlands [2]. Another attractive type of surface for PV installations are roads and highways [3]. In the Netherlands, there are 135,000 km of roads, of which 1,600 km are highways [4], enabling solar power generation on road or highway networks [3] to possibly be a new direction for the energy transition. The integration of PV systems into buildings and other infrastructure such as roads is an increasingly needed area of research as traditional rooftop and solar farm configurations may not be sufficient for land-scarce and population-dense regions to meet renewable energy targets. Current literature [5–7] emphasizes the multifaceted benefits of BIPV, including reduction of material use, dual functionality of existing structures, potential for substantial contributions to local energy needs, noise reduction, cost efficiency and aesthetics, among other advantages. In line with this viewpoint, Heinrich and Forster [8] highlight the utilization of road networks for solar power generation as a strategic response to the rising energy demands in densely populated regions. Furthermore, recent literature is beginning to provide comprehensive and realistic evaluations of energy yield and optimization strategies for PV installations under real irradiance conditions. The work of Pal *et al* develops optimization and enhancement strategies for PV installations exploring the use of bifacial modules and reflectors to enhance energy capture while using spectro-angular irradiance [9–13]. Huyeng *et al* [14] conducted a comparative analysis exploring various technical aspects of road-integrated PV systems, providing insights into the effectiveness of different configurations and their yields. Nevertheless, uncertainties remain about possible yield enhancements through the introduction of reflector surfaces under realistic conditions in particular application settings. The study presented here addresses this gap by using spectro-angular irradiance to investigate the performance of a bifacial PV installation and reflectors

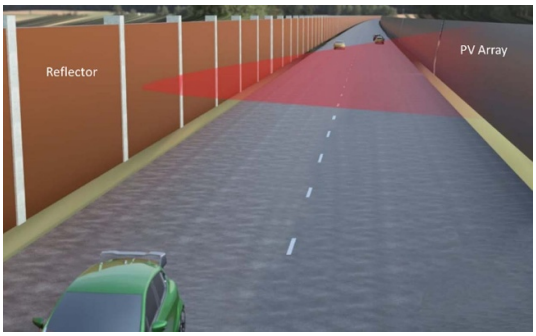

Figure 1. 3D rendering of a reflector façade for a highway sound barrier.

integrated into a highway, offering insights and opportunities for realistic optimizations in the broader context of sustainable energy solutions.

The system investigated here uses bifacial modules as a means to maximize yield [15]. Unlike conventional monofacial modules, bifacial modules capture more irradiance by accepting light from both front and rear sides, leading to typically 4%–15% higher energy yield in large PV solar farms and over 20% in rooftop applications [16, 17], varying with module mounting height, tilt and ground reflectance, i.e. albedo [17–20]. Furthermore, adding reflectors in the vicinity of such structures can increase energy yield [12, 21], depending on their optical properties. The two most common types of reflectors are specular reflectors, such as conventional mirrors, and diffuse/Lambertian reflectors, such as white walls. It is essential to account for the spectral and angular composition of the light incident on the PV modules. The spectro-angular composition of the irradiance in outdoor conditions depends on numerous factors, such as geographical location [22, 23], time of the day and year, climate, weather, cloud coverage [24], atmospheric and environmental conditions, which can cause errors in irradiance modeling and consequently, in PV yield modeling, since the input irradiance directly affects the PV output. Working with precise and high-quality year-long spectro-angular irradiance data in hourly or minute resolution can help solve this problem and improve modeling accuracy.

This study examines the energy yield of a PV installation integrated in a highway in the Netherlands for 2020, both with and without additional reflector irradiance. The arrangement of PV modules takes inspiration from an existing solar highway in Uden, the Netherlands [25]. The spectro-angular irradiance data is computed using a satellite-based irradiance dataset for Cabauw, the Netherlands. A comparison is made between a road-side integrated solar power plant with reflectors (see figure 1) and the same PV system with no such reflector. This evaluation aims to enable realistic optimizations of solar highway and other infrastructure-integrated PV installations.

2. Spectro-angular irradiance data

Studies have demonstrated that neglecting the spectral composition of irradiance can lead to an error in energy yield modeling of up to 15% [11, 26] and ignoring the angle dependence can lead to error in yield estimation of 3.5% [26, 27] for a monocrystalline silicon module. Consequently, accurate analysis of PV performance requires the integration of time-resolved 360° spectro-angular irradiance data, particularly when dealing with bifacial modules and angle-dependent albedo.

Therefore, in this study, we employ a detailed ray tracing model that leverages time-resolved spectro-angular irradiance data generated for Cabauw, Netherlands, as its input. The spectro-angular irradiance data is derived using SunCalculator [28], a specialized tool that computes angular and spectrally time-resolved light sources from solar irradiance measurements.

SunCalculator treats direct and diffuse irradiance separately. Direct irradiance is distributed by the sun's position at each timestep. Diffuse light is distributed across the hemisphere according to empirically established models tailored for both clear-sky and overcast sky conditions, weighted by a cloud opacity factor determined from the measured irradiance values. The azimuth angles vary from 0° to 360°, and the altitude angles vary from 0° to 90°, as illustrated in figure 2. Spectral distributions in SunCalculator are based on the SMARTS model [29, 30] considering the sun's elevation angle and assuming standard atmospheric conditions that reproduce the AM1.5G spectrum.

In this paper, we source satellite-derived global horizontal, direct normal, and diffuse horizontal irradiance data for the year 2020 in Cabauw, Netherlands [31]. From this dataset we generate spectro-angular

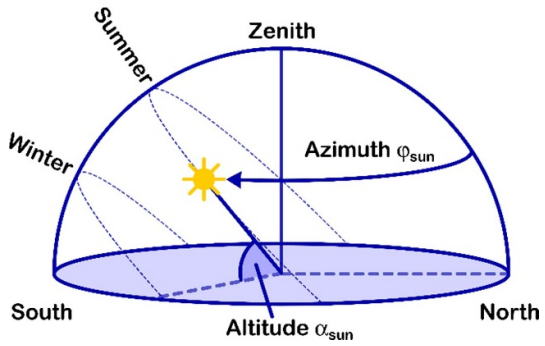

Figure 2. Zenith and azimuth angles from the observer point of view as defined in [28].

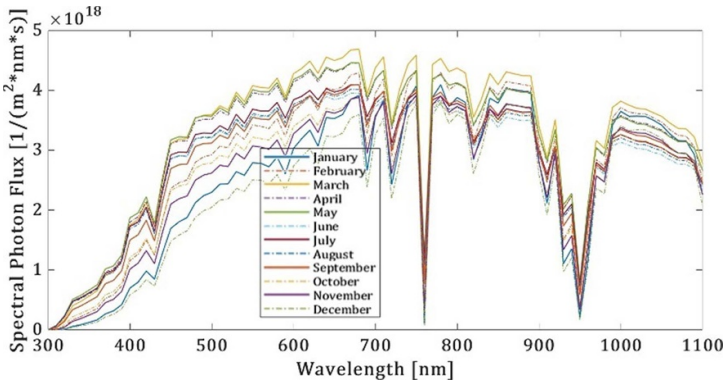

Figure 3. Spectral photon flux for the day with maximum direct irradiance for each month of the year 2020.

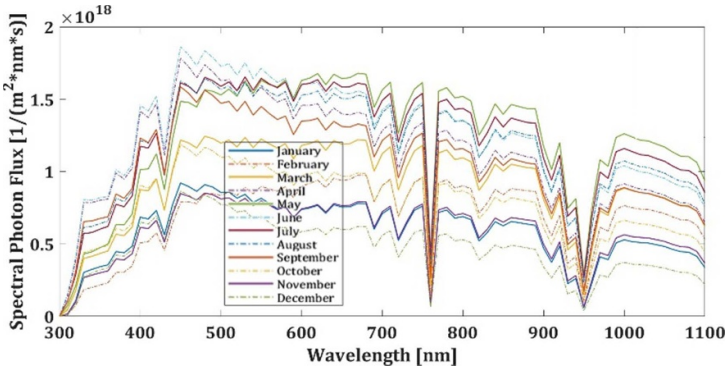

Figure 4. Spectral photon flux for the day with maximum diffuse irradiance for each month of the year 2020.

data with a time resolution of 15 min, an angular resolution of 5°, and a spectral resolution of 10 nm. The spectral irradiance wavelengths for both direct and diffuse irradiance angular distribution range from 300 nm to 1100 nm.

2.1. Monthly irradiance spectrum variation

To gain a comprehensive understanding of the available solar resource throughout the year, we examine the monthly variation in the spectral irradiance, both direct and diffuse, for year 2020 in the Netherlands. In order to visualize the considerable variations in the irradiance spectra throughout the year, we selected the spectra of the day with the highest direct irradiance during solar noon for each month, as well as the spectra of the day with the highest diffuse irradiance during solar noon of each month, as shown in figures 3 and 4, respectively. The day with the highest direct irradiance in each month was determined by selecting the spectrum with the highest solar noon direct peak value. Similarly, the day with the highest diffuse irradiance was determined by selecting the spectrum with the highest solar noon diffuse peak value.

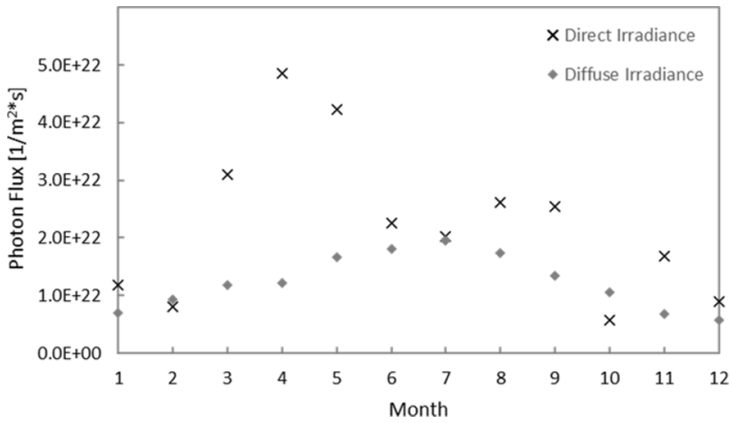

Figure 5. Total integrated photon flux for each month of the year 2020, in the Netherlands for direct (crosses) and diffuse (diamonds) irradiance.

In both scenarios, we observe the expected trend of higher irradiance during summer months and lower irradiance levels during winter months. The spectral distribution remains relatively constant throughout the year. Days with the highest direct irradiance have a peak value of about 2.5 times greater than days with the highest diffuse irradiance. Not only do we observe a clear difference in magnitude between the irradiance spectra for direct and diffuse irradiance, but also a difference in the spectral content of their curves. Cloud scattering [19] causes the peak wavelength range for diffuse irradiance to be shorter (around 470 nm) compared to direct irradiance (around 680 nm). Finally, figure 5 shows the total integrated diffuse and direct irradiance for all the wavelengths and months. Based on the data showing the integrated direct irradiance, the sunniest month in the Netherlands in 2020 was April, during spring, whereas the least sunny month was December, during winter. The integrated diffused irradiance shows an overall trend of higher values during the summer than in winter. This trend is expected since winter days are shorter and the air mass is larger, increasing the distance that light has to travel through the atmosphere.

Since incoming radiation fluctuates throughout the year, these variations should be considered when calculating solar power output. Conducting continuous spectral measurements is a crucial step to gain better understanding of irradiance changes and their impact on PV output, as explained in the introduction. Furthermore, angle-dependent irradiance plays an important role, particularly in bifacial installations. Hence, our study incorporates spectrum and angle-resolved irradiance data.

3. System design

This paper examines four BIPV configurations with vertically mounted bifacial PV modules as sound barriers on a highway. One of the configurations is a no-reflector system, while the other configurations contain vertically wall-integrated ideal specular, diffuse or black reflector facing the bifacial modules. We consider a reflector diffuse or specular based on the size of its reflection lobe. Specular reflectors have a sharp peak in the reflection lobe [32]. Mathematically, specular reflection R_S is defined as:

$$R_S = \frac{\delta(\theta_i - \theta_r)\,\delta(\phi_i - \phi_r)}{\cos\theta_r},$$

where θ and ϕ are the zenith and azimuth angles, respectively, according to the spherical coordinate system. $\delta(\theta_i - \theta_r)$ is the Dirac delta distribution, the subscripts i and r denote the direction of the incidence and reflection.

Diffuse reflectors have a uniformly distributed lobe [32], mathematically defined as:

$$R_D = \frac{1}{\pi}.$$

An ideal diffuse reflector is also known as a Lambertian reflector. The choice of considering reflection lobe sizes as a basis for categorizing reflectors aligns with established practices in optical design and photometry. In optical engineering, the reflection characteristics of surfaces are often analyzed based on the angular distribution of reflected light. Specular reflectors, such as conventional mirrors, exhibit a distinct peak in their reflection lobe, resulting in concentrated reflections at specific angles. In contrast, diffuse reflectors, or Lambertian surfaces, scatter light uniformly across a range of angles, lacking a pronounced peak

in their reflection lobe. More information on different types of reflectors and their influence on bifacial solar cell output can be found in [13]. This paper uses ideal specular, diffuse, and black wall reflectors. We focus on the angle dependent reflection properties and assume the spectral behavior to be constant, i.e. we assume unity reflectivity for the ideal specular and diffuse reflector and zero reflectivity for the black wall across the whole spectrum respectively. It should be noted that the black reflector represents the worst-case scenario of a dark wall opposite the PV modules.

The module configuration is inspired by an existing solar highway in the Netherlands [25]. This solar highway is located in the north-south stretch of the A50 motorway near Uden, the Netherlands, and uses bifacial PV modules with an east-west configuration as its solar sound barrier. Since the sound barrier is placed adjacent to a road next to a residential zone, its primary functions are to provide green energy to the residential zone and to protect the inhabitants from the excessive noise levels of the highway. The solar sound barrier consists of 268 solar modules (laminates) designed by ECN [25], each being 3 meters wide and 2 meters high. Two modules are framed together and made into a cassette and two cassettes are placed on top of each other between poles to form a section [25].

The physical extent of this prototype spans 400 m in lengths of the 5 m high noise barrier with 4 m high fully integrated bifacial PV modules. Hence, the PV modules cover a total area of 1600 m^2. The solar sound barrier is deliberately tilted 10° towards the east side (see figure 6(a))since the front face was mounted to face west. Therefore, the slope increases accumulated annual yield from the front side such as it is the case for conventional monofacial solar power plants.

The near-vertical tilt of the PV modules minimises the accumulation of dust and particles, further aided by natural self-cleaning during rainfall [25]. Since the positioning of the PV modules is based on an existing setting, our analysis focusses on investigating the impact of introducing a reflector system.

Given the highway's orientation from north to south and the west-facing alignment of the bifacial vertical PV modules, a vertical reflector wall surface is positioned to face east. This arrangement maximizes the sunlight absorption and redirection from both the PV modules and the reflectors throughout the day. Furthermore, such a structure would also serve as an additional sound barrier on the opposite side of the road. Figure 1 shows a visual representation of the complete system with PV modules as the sound barrier alongside the reflector façade positioned opposite and figure 6 shows a schematic including some angles and specific incident irradiance directions.

It is important to note that the distance between the reflector and solar modules discussed in this analysis was chosen as a starting point but ought to be adjusted to the specific requirements of the highway studied.

4. Output enhancement by optimized reflectors façade

To simulate and assess the performance of the four reflector cases, this paper uses a 3D reverse ray tracing software [12]. In this method, light is treated as rays originating from an incoherent source and interacting with objects in a ray optical manner. To save on computational time, reverse ray tracing is employed here. This means that the rays start from the solar module and are followed backwards until they reach the source. Thereby, only rays that actually end up on the solar module have to be calculated instead of calculating all rays originating from the source. Further details about this software can be found in [12]. The short-circuit current density (J_{sc}) including the effects of angle of incidence (AoI) and shading are simulated with this software. It is assumed that all photons absorbed in the solar cell's absorber layer contribute to J_{sc}. In other words, the internal quantum efficiency is set to be unity, which is a reasonable assumption for high quality silicon solar cells. Spectro-angular irradiance data as explained in section 2 was used as the input irradiance. The incoming irradiance is assumed to consist of parallel rays under each respective AoI. Albedo from the surroundings such as the road and the east side of the solar modules were neglected in this study. For the module, a silicon heterojunction bifacial module, with bifaciality = 98.8% was used [33]. We assumed a constant open circuit voltage of 0.73 V and fill factor of 0.85 to determine the power output and energy yield respectively. Mismatch losses due to inhomogeneous module illumination were neglected in this study, but the ray tracing software is able to handle these as well.

5. Energy yield

To evaluate the profitability of the configurations, we calculate the total energy output (E_t) in kWh m^{-2}. The results for various sound barrier-integrated configurations during the year 2020 in the Netherlands are shown in figures 7–10. The relative enhancements compared to a no-reflector system and black wall reflector are calculated and given in table 1.

Figure 7 shows E_t of a PV system with no reflector. The daily energy output due to direct irradiance is shown in blue, while the daily energy output due to diffuse irradiance is shown in red. Days 61–152 represent

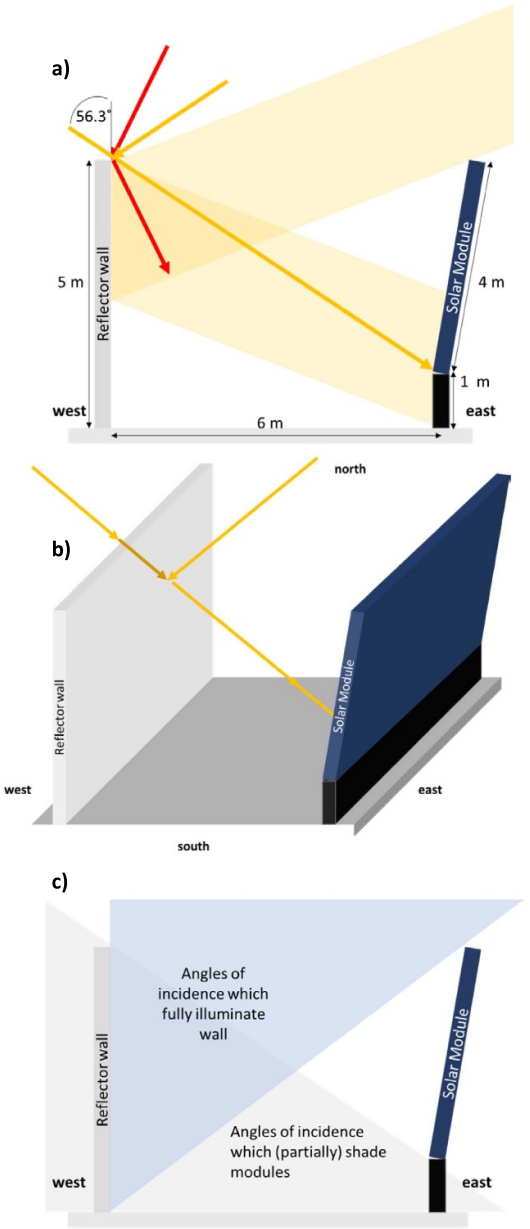

Figure 6. (a) Shading and reflection conditions dependent on the zenith angle for a specular reflector. (b) Schematic of a ray incident from north-west being compensated by the symmetrical ray incident from north-est. (c) Schematic of the angles of incidence causing shading and reflection in the case of a diffuse reflector.

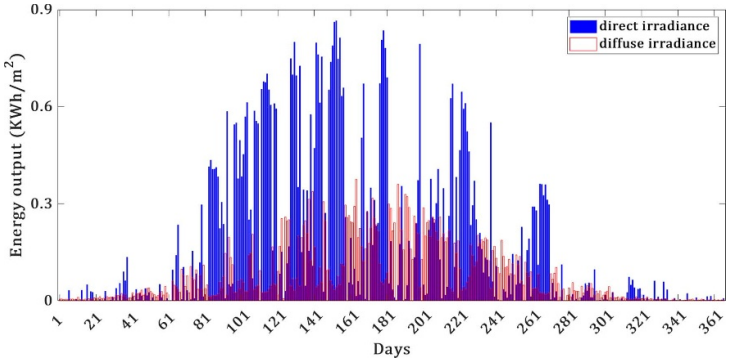

Figure 7. Daily energy output per m^2 of the PV system with no reflector in 2020.

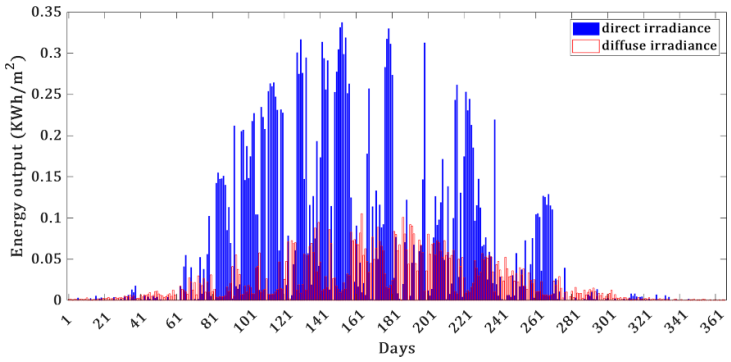

Figure 8. Daily energy output per m^2 of the PV system with black reflector wall in 2020.

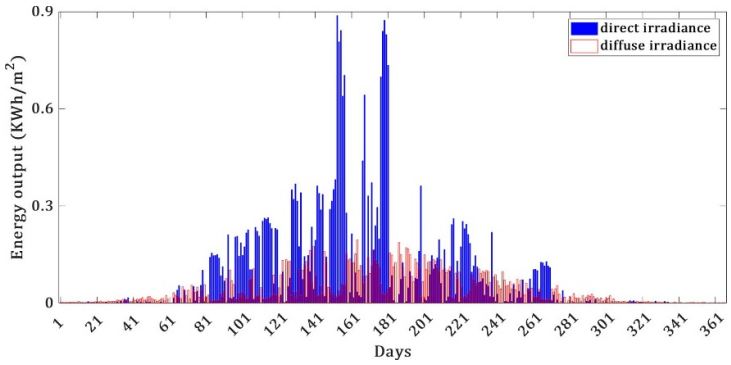

Figure 9. Daily energy output per m^2 of the PV system with specular reflector wall in 2020.

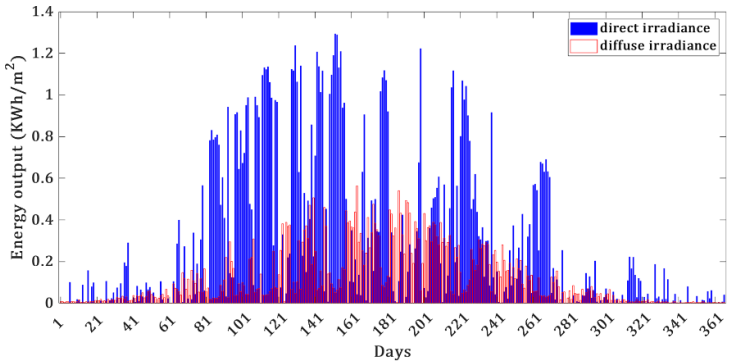

Figure 10. Daily energy output per m^2 of the PV system with a Lambertian reflector wall in 2020.

Table 1. Gains and losses induced by walls with different types of reflectors compaired to no reflector and a black wall reflector.

	No reflector	Black (wall) reflector
Black (wall) reflector	−62.6%	0%
Specular reflector	−49.2%	+35.9%
Lambertian reflector	+70%	+354.5%

the spring season, 153–244 the summer season, 245–335 the autumn season, and 336–60 the winter season, in the Netherlands. The highest energy output contribution clearly comes from the spring and summer months, with spring having the highest yield for the year 2020, while autumn and winter seasons have a much lower energy output. As expected, the energy yield contribution from direct light is generally higher than that of diffuse light, as shown in sections 2 and 2.1. Days with direct irradiance lower than diffuse irradiance indicate days with high cloud cover. An example of such occurrence is day 41, which corresponds

to February 10th. Based on figure 5, it is evident that the total diffuse irradiance during February is higher than the total direct irradiance for the same month. Days 62, 124, 186 seemingly have the lowest total irradiance. This is due to high cloud cover, and low sun-hours in the Netherlands during these days [34].

Figure 8 shows the daily energy output of the PV system with an ideal black wall, meaning this wall does not reflect any light. It is observed that although the shape of the curve in figure 8 is similar to the scenario without reflector shown in figure 7, there has been a significant reduction in magnitude. This is due to the shading effects produced by the black wall, which is absent in the no-reflector case. Since the wall does not reflect any light, it does not enhance the energy generation of the PV modules, but rather diminishes it.

In figure 9, the results for the specular reflector are shown. Overall, the specular reflector leads to a higher yield than a black reflector since it can compensate for some shading conditions. In figures 6(a) and (a) 2-dimensional representation of the system is shown. Shading occurs for zenith angles larger than 56.3° for rays from the western hemisphere. Some of the shading is compensated by rays from the opposite direction in the eastern hemisphere and specularly reflected at the wall, as illustrated by the yellow ray. For rays with smaller zenith angle, there is no shading, but the specular reflector also does not add anything to the yield (see red ray). Between 56.3° and approximately 90° zenith angle, some rays incident from the western hemisphere that are blocked by the wall can be compensated by the symmetrical rays from the eastern hemisphere, therefore, the overall yield of the specular reflector is higher than that of a black wall. This situation is shown by the yellow shaded area in figure 6(a). The greater the zenith angle, the smaller the area on the reflector wall which can contribute to the reflection since the solar modules lead to shading of the wall. On the other hand, the smaller the zenith angle, the more rays will be redirected towards the road in between wall and modules since their angle of incidence is too steep. A special situation occurs for a number of days around the summer solstice. During these days, the specular wall yields the same output as no wall. The wall does not cast any shadow, since rays originating from south-west angles always have zenith angles smaller than 56.3°. Rays originating from north-west angles which cast a shadow on the solar modules are fully compensated by their symmetrical twins from the north-east direction by the specular mirror. This is schematically shown in figure 6(b).

The resulting daily energy yield for a Lambertian reflector wall is shown in figure 10. It can be seen that the results not only surpass that of the black wall, but also yield higher output than a situation without a reflector wall. We observe a relative total yield enhancement of 70% as opposed to a no-reflector system and a relative enhancement of 354.4% as compared to an ideal black wall, which redirects no light. Contrary to the specular reflector, every ray that hits the Lambertian wall reflector, will be partially reflected towards the solar modules since the direction will be randomized. Therefore, in this configuration, the Lambertian overall performs better than the specular reflector. Moreover, the shading will be even overcompensated since the angles of incidence from the western hemisphere which are blocked by the wall contain less intense light than the benefit resulting from the Lambertian reflection. In other words, the Lambertian reflector allows solar modules to gain a wider range of viewing angles from the eastern hemisphere, outweighing the loss in viewing angles from the western hemisphere. This is schematically shown in figure 6(c).

For all the systems, the highest energy daily output occurs during May, followed by a second high peak in June. This is due to the position of the sun (azimuth and elevation angles) being more favorable in those months for the configuration used here. Furthermore, the summer solstice 'the longest day of the year' occurs in June, meaning that there are more sun hours available, causing much higher current density generation due to PV modules and reflectors. The lowest energy producing month in all the systems is the month of December. Here the winter solstice 'the shortest day of the year' occurs, and the sun's elevation and azimuth angles are not favorable for a high energy output generation.

In figures 11 and 12 we directly compared the daily energy output per m^2 of all the configurations, due to direct and diffuse irradiance, respectively. The trends described above can be directly compared in these graphs. It can be seen that the black wall significantly reduces the yield for both direct as well as diffuse light. It should be noted that such a reduction would not only occur by a deliberately placed wall, but hedges and trees across the PV modules could also lead to a partial yield reduction due to shading. The specular reflector behaves very similar to the black wall, only for certain days during the summer can it compensate the shading as explained above. The Lambertian reflector wall provides significant yield enhancement for both diffuse as well as direct light. Most importantly, it should be noted that a Lambertian reflector significantly enhances the yield during winter, making such a configuration highly beneficial to improve energy demand and supply matching.

In reality, no reflector inhibits unity reflectance across the full spectrum. A realistic white wall has a 80%–90% reflectance across the visible regime. The enhancement values would have to be scaled with the real reflectance to determine the yield with a realistic wall. Furthermore, all materials have a wavelength dependence in their reflectance. If the reflectance is not uniform across the visible spectrum, the material will display a certain color. Uniform reflectance across the whole visible spectrum appears as different shades of

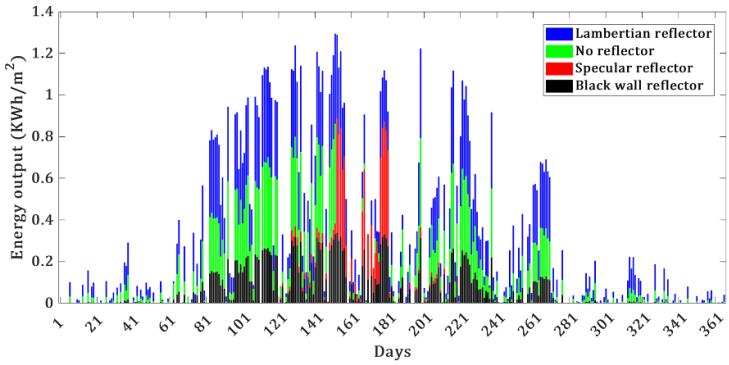

Figure 11. Daily energy output per m^2 of all configurations, during 2020 due to direct irradiance.

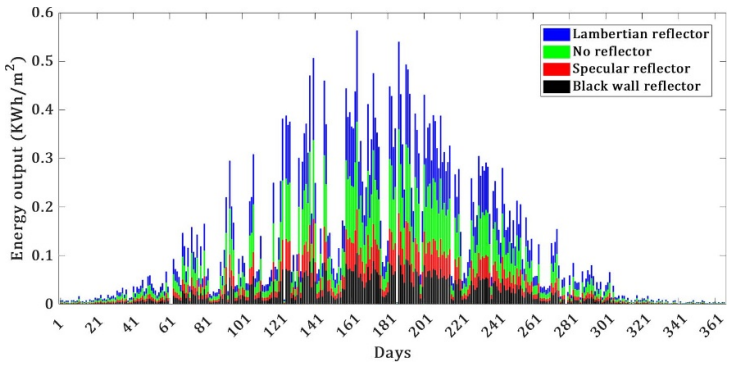

Figure 12. Daily energy output per m^2 of all configurations, during 2020 due to diffuse irradiance.

grey. With our software, such wavelength dependences are easily implemented since the software calculates the yield for each wavelength individually.

6. Assumptions and limitations

To focus on the effect of adding reflectors to PV power plants under realistic irradiance conditions while keeping computational time reasonable, we made several assumptions. First, we assumed that the reflectors that we added have either unity or zero (black wall) reflectance across the whole spectrum. Therefore, the results present best and worst case scenarios. It is straightforward to scale the results for different types of grey reflectors. Reflectors with a wavelength dependent reflectance, i.e. all colored reflectors, require to treat each wavelength separately. Our software is designed for such studies and only requires the wavelength dependent reflectance as an input [12]. As a further assumption, we neglected albedo from all surroundings other than the reflector wall. In other words, the road, cars passing by and the land east of the solar modules were assumed to be black. In reality, these surroundings also add some irradiance and therefore, increase the yield. The influence on the enhancement or reduction by adding the reflector wall is negligible though, thereby, the conclusions drawn in this study remain unaffected by this assumption. A third assumption is that the solar modules operate with constant open circuit voltage and fill factor. In reality, both these values are affected by the short circuit current as well as by the temperature. Since the temperature is heavily dependent on ambient temperature and wind load, we opted to keep these values constant, but for a more accurate treatment, these dependences should be included. Finally, we did not include mismatch losses that result from uneven illumination of the modules. Our software can give us information on the distribution of the illumination and in a previous study, we have seen, that the mismatch is particularly pronounced when introducing specular reflectors [13]. Here, we assumed that all photons reaching the module contribute to the yield independent of the homogeneity of the illumination. In reality, the yield will heavily depend on the wiring of the cells and the modules. For a more accurate description of a specific system, uneven illumination and resulting mismatch losses should be analyzed.

7. Conclusion

In this paper we analyzed the yield of a road-integrated bifacial solar power system used as a sound barrier on the east side of a highway in the Netherlands. Using inverse 3D ray tracing, we simulated the changes in yield that occur when a sound barrier with different reflectors is added to the other side of the road. Using spectrum and angle resolved irradiance data for 2020, we calculated the yield for a configuration with no additional sound barrier and for sound barriers with black, ideal specular, and ideal diffuse reflectors respectively. Our calculations show an annual yield enhancement of 35.9% for specular reflector, relative to an ideal black reflector (representing the worst-case scenario), but also show that adding a specular reflector sound barrier reduces the overall annual system yield by 49.2%. This reduction arises from the shadow which the additional sound barrier casts onto the bifacial solar modules. However, the Lambertian reflector leads to a relative yield enhancement of 70% and 354.5%, compared to no additional sound barrier and compared to the black reflector case, respectively. Most notably, the energy yield is significantly increased during the winter months. This shows that strategically placing reflectors in the vicinity of infrastructure integrated solar power installations can increase the annual yield and help close the gap between summer and winter production. With increasing solar penetration, distributing solar production over the course of the year and in particular, increasing production during the winter is becoming more and more important. Our study shows that vertical bifacial installations in combinations with reflectors have great potential to solve this challenge and should be further investigated to increase the value of solar installations.

Data availability statement

All data that support the findings of this study are included within the article (and any supplementary files).

Acknowledgments

This publication is part of the project Diffuse Irradiance Redirector for Efficient ConcenTration (DIRECT) with Project Number KICH1.ED02.20.006 of the research programme KIC Innovations for Wind and Solar Energy which is financed by the Dutch Research Council (NWO).

ORCID iDs

Shweta Pal https://orcid.org/0000-0001-6990-8226
Marco Ernst https://orcid.org/0000-0003-2556-6943
Rebecca Saive https://orcid.org/0000-0001-7420-9155

References

[1] SolarNL 2023 SolarNL.eu
[2] CBS Zonnestroom; vermogen en vermogensklasse, bedrijven en woningen, regio (available at: https://opendata.cbs.nl/#/CBS/nl/dataset/85005NED/table) (Accessed 23 August 2023)
[3] TNO Solar panels on and along the road (available at: www.tno.nl/en/sustainable/renewable-electricity/solar-safety/solar-panels-road/#:~:text=Solar%20Highways%20is%20a%20noise,Heijmans%20Infra%20built%20the%20barrier.) (Accessed 23 August 2023)
[4] Wassink J Solar highways: why the first one will be a cycle path (available at: www.delta.tudelft.nl/article/solar-highways-why-first-one-will-be-cycle-path#) (Accessed 23 August 2023)
[5] Forster J, Tsutskiridze G, Herr C, Huyeng J, Basler F, Kohlhauer R, Neuhaus D H, Heinrich M and Rendler L C 2023 Photovoltaic noise barriers as energy generating infrastructure: functional overview about five solutions (available at: https://publica-rest.fraunhofer.de/server/api/core/bitstreams/2e07a775-a4ed-4a4e-b210-a2f9c8245262/content)
[6] Zomer C, Nobre A, Cassatella P, Reindl T and Rüther R 2014 The balance between aesthetics and performance in building-integrated photovoltaics in the tropics *Prog. Photovolt., Res. Appl.* **22** 744–56
[7] Awuku S A, Muhammad-Sukki F and Sellami N 2022 Building integrated photovoltaics—The journey so far and future *Book Building Integrated Photovoltaics—The Journey so Far and Future* (MDPI) p 1802
[8] Heinrich M and Forster J 2022 Road infrastructure integrated photovoltaics—Equipping noise barriers or road canopies with solar (available at: www.delegacionuenavarra.es//uploads/files/220530_RIPV_Fraunhofer_Navarre_Martin_Heinrich.pdf)
[9] Pal S and Saive R 2021 Output enhancement of bifacial solar modules under diffuse and specular albedo *Book Output Enhancement of Bifacial Solar Modules under Diffuse and Specular Albedo* (IEEE) pp 1159–62
[10] Pal S S and Saive R 2019 Experimental study of the spectral and angular solar iirradiance *Book Experimental Study of the Spectral and Angular Solar Iirradiance* (IEEE)
[11] Pal S, Reinders A and Saive R 2020 Simulation of bifacial and monofacial silicon solar cell short-circuit current density under measured spectro-angular solar irradiance *IEEE J. Photovolt.* **10** 1803–15
[12] Pal S 2022 Tracing the light: designing reflectors for bifacial photovoltaic yield enhancement under outdoor irradiance *PhD Thesis* University of Twente
[13] Pal S S, van Loenhout F H, Westerhof J and Saive R 2023 Understanding and benchmarking ground reflectors for bifacial photovoltaic yield enhancement *IEEE J. Photovolt.* **14** 160–9

[14] Huyeng J, Forster J, Basler F, Romer P, Beinert A, Schill C, Heinrich M, Neuhaus H and Wirth H 2022 Technical aspects for road integrated photovoltaics towards a more sustainable mobility sector (available at: https://publica-rest.fraunhofer.de/server/api/core/bitstreams/a754215b-4bce-4fb8-8044-b09cd1f9a874/content)
[15] Deline C A, Ayala Pelaez S, Marion W F, Sekulic W R, Woodhouse M A and Stein J 2019 Bifacial PV system performance: separating fact from fiction *Book Bifacial PV System Performance: Separating Fact from Fiction* (National Renewable Energy Lab.(NREL))
[16] Byrne J, Nyangon J, Hegedus S, Chajes M, Taminiau J, Ahmed N, Dinardo N, Li P and Xu J 2019 Feasibility study of city-scale solar power plants using public buildings: case studies of newark and wilmington delaware with early investigations of bifacial solar modules and dual orientation racking as tools for city-scale solar development *Book Feasibility Study of City-Scale Solar Power Plants Using Public Buildings: Case Studies of Newark and Wilmington Delaware with Early Investigations of Bifacial Solar Modules and Dual Orientation Racking as Tools for City-Scale Solar Development* (Technical report prepared for the Delaware General Assembly)
[17] Pelaez S A, Deline C, Greenberg P, Stein J S and Kostuk R K 2019 Model and validation of single-axis tracking with bifacial PV *IEEE J. Photovolt.* **9** 715–21
[18] Patel M T, Ahmed M S, Imran H, Butt N Z, Khan M R and Alam M A 2021 Global analysis of next-generation utility-scale PV: tracking bifacial solar farms *Appl. Energy* **290** 116478
[19] Ernst M, Conechado G E and Asselineau C-A 2021 Accelerating the simulation of annual bifacial illumination of real photovoltaic systems with ray tracing *iScience* **25** 1
[20] Ernst M, Liu X, Asselineau C-A, Chen D, Huang C and Lennon A 2024 Accurate modelling of the bifacial gain potential of rooftop solar photovoltaic systems *Energy Convers. Manage.* **300** 117947
[21] Einhaus L M, Heres G C, Westerhof J, Pal S, Kumar A, Zheng J-Y and Saive R 2023 Free-space diffused light collimation and concentration *ACS Photonics* **10** 508–17
[22] Gottschalg R, Betts T, Infield D and Kearney M 2005 The effect of spectral variations on the performance parameters of single and double junction amorphous silicon solar cells *Sol. Energy Mater. Sol. Cells* **85** 415–28
[23] Lave M, Hayes W, Pohl A and Hansen C W 2015 Evaluation of global horizontal irradiance to plane-of-array irradiance models at locations across the United States *IEEE J. Photovolt.* **5** 597–606
[24] Pfister G, McKenzie R, Liley J, Thomas A, Forgan B and Long C N 2003 Cloud coverage based on all-sky imaging and its impact on surface solar irradiance *J. Appl. Meteorol. Climatol.* **42** 1421–34
[25] TNO Solar Highways Monitoring (available at: www.solarhighways.eu/en/document/monitoring-end-report/) (Accessed 23 August 2023)
[26] Lindsay N, Libois Q, Badosa J, Migan-Dubois A and Bourdin V 2020 Errors in PV power modelling due to the lack of spectral and angular details of solar irradiance inputs *Sol. Energy* **197** 266–78
[27] Martín N and Ruiz J 2005 Annual angular reflection losses in PV modules *Prog. Photovolt., Res. Appl.* **13** 75–84
[28] Ernst M, Holst H, Winter M and Altermatt P P 2016 SUNCALCULATOR: A program to calculate the angular and spectral distribution of direct and diffuse solar radiation *Sol. Energy Mater. Sol. Cells* **157** 913–22
[29] Gueymard C 1995 *SMARTS2: A Simple Model of the Atmospheric Radiative Transfer of Sunshine: Algorithms and Performance Assessment* (Florida Solar Energy Center)
[30] Gueymard C A 2001 Parameterized transmittance model for direct beam and circumsolar spectral irradiance *Sol. Energy* **71** 325–46
[31] Solcast 2020 Solar Irradiance Data (available at: https://solcast.com) (Accessed 23 August 2023)
[32] Regan M and Pose R 1994 Priority rendering with a virtual reality address recalculation pipeline *Book Priority Rendering with a Virtual Reality Address Recalculation Pipeline* (Association for Computing Machinery) pp 155–62
[33] Russell T C, Saive R, Augusto A, Bowden S G and Atwater H A 2017 The influence of spectral albedo on bifacial solar cells: a theoretical and experimental study *IEEE J. Photovolt.* **7** 1611–8
[34] KNMI Klimatologie—Overzichten (available at: www.knmi.nl/nederland-nu/klimatologie-overzichten) (Accessed 23 August 2023)